Quantifying epigenetic modulation of nucleosome breathing by high-throughput AFM imaging

Sebastian F. Konrad, Willem Vanderlinden, Jan Lipfert

Angaben zur Veröffentlichung / Publication details:

Konrad, Sebastian F., Willem Vanderlinden, and Jan Lipfert. 2022. "Quantifying epigenetic modulation of nucleosome breathing by high-throughput AFM imaging." *Biophysical Journal* 121 (5): 841–51. https://doi.org/10.1016/j.bpj.2022.01.014.

Biophysical Journal
Article

Biophysical Society

Quantifying epigenetic modulation of nucleosome breathing by high-throughput AFM imaging

Sebastian F. Konrad,[1] Willem Vanderlinden,[1] and Jan Lipfert[1,*]
[1]Department of Physics and Center for NanoScience, LMU Munich, Munich, Germany

ABSTRACT Nucleosomes are the basic units of chromatin and critical for storage and expression of eukaryotic genomes. Chromatin accessibility and gene readout are heavily regulated by epigenetic marks, in which post-translational modifications of histones play a key role. However, the mode of action and the structural implications at the single-molecule level of nucleosomes is still poorly understood. Here we apply a high-throughput atomic force microscopy imaging and analysis pipeline to investigate the conformational landscape of the nucleosome variants three additional methyl groups at lysine 36 of histone H3 (H3K36me3), phosphorylation of H3 histones at serine 10 (H3S10phos), and acetylation of H4 histones at lysines 5, 8, 12, and 16 (H4K5/8/12/16ac). Our data set of more than 25,000 nucleosomes reveals nucleosomal unwrapping steps corresponding to 5-bp DNA. We find that H3K36me3 nucleosomes unwrap significantly more than wild-type nucleosomes and additionally unwrap stochastically from both sides, similar to centromere protein A (CENP-A) nucleosomes and in contrast to the highly anticooperative unwrapping of wild-type nucleosomes. Nucleosomes with H3S10phos or H4K5/8/12/16ac modifications show unwrapping populations similar to wild-type nucleosomes and also retain the same level of anticooperativity. Our findings help to put the mode of action of these modifications into context. Although H3K36me3 likely acts partially by directly affecting nucleosome structure on the single-molecule level, H3S10phos and H4K5/8/12/16ac must predominantly act through higher-order processes. Our analysis pipeline is readily applicable to other nucleosome variants and will facilitate future high-resolution studies of the conformational landscape of nucleoprotein complexes.

SIGNIFICANCE Packing and readout of our genome are tightly regulated by post-translational modifications (PTMs). Although a vast range of PTMs has been studied with respect to their implications for gene activity and replication, a detailed view of the direct effect of PTMs on conformational changes of nucleosomes is still lacking. Here we investigate the structural implications of several key modifications (three additional methyl groups at lysine 36 of histone H3, phosphorylation of H3 histones at serine 10, and acetylation of H4 histones at lysines 5, 8, 12, and 16) by high-throughput AFM imaging. Our findings enable a better understanding of the mode of action of these specific modifications and provide an analysis pipeline for the investigation of other epigenetic modifications.

Nucleosomes are the fundamental units of compaction of eukaryotic DNA into chromatin and function as regulators of gene readout and activity (1–3). Canonical nucleosome core particles consist of two copies each of the four histones H2A, H2B, H3, and H4, assembled into a histone octamer that is wrapped by ~147 bp of DNA (4,5). Electrostatic interactions and specific molecular contacts stably pack the DNA onto the histone octamer, but DNA breathing, sliding, gaping, and loosening allow nucleosomal dynamics at the millisecond to minute timescales (6–9).

Post-translational modifications (PTMs) of histones play a key role in formation of higher-order chromatin structure (3,10–14), recruitment of proteins and complexes with specific enzymatic activities (15), and maintenance of DNA repair (16) and replication (17). Numerous histone variants and PTMs alter histone-histone and histone-DNA interactions (18–20) to yield nucleosomal structures with varying degrees of stability and DNA wrapping. Specifically, PTMs at the N-terminal tails of histones H3 and H4, located next to the DNA entry/exit sites, can affect DNA opening dynamics by introducing an additional charge, neutralizing an existing charge, or adding steric constraints (2,21). Among the astonishing number of PTMs (22,23), the most frequent PTMs at the histone-DNA interface are methylations, acetylations, and phosphorylations (2,15). Acetylation

Submitted July 27, 2021, and accepted for publication January 19, 2022.
*Correspondence: jan.lipfert@lmu.de
Editor: Tom Misteli.
https://doi.org/10.1016/j.bpj.2022.01.014

neutralizes the positive charge of lysine, and phosphorylation introduces a negative charge. Methylation does not alter the charge of the histone protein but, similar to acetylation and phosphorylation, adds steric bulk to the system.

Although many studies have investigated PTMs with respect to their effects on nucleosomal structural dynamics (24,25) and on the interaction with nucleosome- or DNA-binding proteins (26–28), a detailed investigation of the effect of distinct PTMs on nucleosome wrapping is currently lacking. It is critical to understand the direct effects of PTMs on nucleosome conformations because they can influence the accessibility of nucleosomal DNA for readout and processing and can modulate the conformational landscape that underlies interactions with additional binding partners.

Here we use a high-throughput pipeline based on atomic force microscopy (AFM) imaging to investigate the conformational landscape of nucleosome variants with several key post-translational N-terminal tail modifications on histones H3 and H4: three additional methyl groups at lysine 36 of histone H3 (H3K36me3), phosphorylation of H3 histones at serine 10 (H3S10phos), and acetylation of H4 histones at lysines 5, 8, 12, and 16 (H4K5/8/12/16ac) (Fig. 1 *a*). These specific modifications are selected for several reasons. First, our goal is to investigate a range of different nucleosome modifications and, therefore, cover trimethylation, acetylation, and phosphorylation. Second, we aim for modifications at different positions in the histones. Although H3K36me3 and H4K5/8/12/16ac lie close to the DNA entry/exit region of histones H3 and H4, respectively, H3S10phos is located more distally toward the start of the N-terminal tail of histone H3. Third, for H3K36me3 (29,30) and H4K5/8/12/16ac (31), previous measurements of the nucleosome structure found no direct effect of the modifications. However, because of the close proximity of both modifications to the DNA entry/exit site, we hypothesized that these PTMs could have an effect on the nucleosome wrapping landscape and aimed to detect it with our sensitive assay. Likewise, H3S10phos is an interesting modification because it is involved in transcriptional activation and chromatin compaction (32), two structurally opposed processes, therefore raising the question whether H3S10phos has structural implications for the nucleosome itself or merely acts as a protein binding platform.

AFM imaging is a powerful tool to probe DNA and nucleosome structure (33–40), and we have recently developed a multiparameter image analysis pipeline to quantify the wrapping of nucleosomes with nanometer resolution, label free, and at the single-molecule level (39). Here we improved the resolution of our assay by adding a deconvolution step to allow more accurate parameter tracing, enabling direct observation of the nucleosomal unwrapping periodicity of 5 bp from nucleosomal opening angles. We find that nucleosomes with the H3K36me3 modification are significantly less likely to occur in the fully wrapped state compared with canonical nucleosomes and to exhibit stochastic instead of anticooperative unwrapping. In contrast, H4K5/8/12/16ac and H3S10phos do not show significant changes in unwrapping or anticooperativity compared with canonical nucleosomes. We discuss these results in the context of biological function and epigenetic regulation of genome organization.

MATERIALS AND METHODS

DNA purification and nucleosome reconstitution

DNA was PCR amplified from a GeneArt High-Q String DNA fragment (Thermo Fisher Scientific, Waltham, Massachusetts) containing the Widom 601 positioning sequence. The DNA was purified using a QIAquick PCR purification kit (Qiagen, Hilden, Germany) and subsequently eluted to a volume of 30 μL in milliQ water. Unmodified and modified histone proteins were purchased from EpiCypher (Durham, NC). Nucleosome reconstitution was performed by salt gradient dialysis (41). The dialysis chambers contained 0.65 μg of the histone octamers and 3 μg of the 486-bp DNA at 2 M NaCl and were placed in 1 L of high-salt buffer (2 M NaCl, 10 mM Tris, 1 mM EDTA). Over the course of 15 h, 3 L of low-salt buffer (50 mM NaCl, 10 mM Tris, 1 mM EDTA) were transferred to high-salt buffer at 4°C. Finally, the dialysis chambers were moved to 1 L of low-salt buffer for 3 h. The resulting nucleosome samples were tested using gel electrophoresis (Fig. S7). We used a 1% agarose gel in 0.2× TBE (Tris/Borate/EDTA, pH 8.0) gel/running buffer. The loading dye contained 30% glycerol and 10 mM Tris. 70 V was applied to the 10-cm gel for a total of 60 min in a cold room (4°C), and then the gel was stained in ethidium bromide for 15 min with subsequent destaining in milliQ water for 10 min.

AFM sample preparation and imaging

Poly-L-lysine-coated mica was prepared by depositing 20 μL poly-L-lysine (0.01% w/v) on freshly cleaved muscovite mica for 30 s and subsequently rinsing the surface with 50 mL of milliQ water before drying with a gentle stream of filtered N_2 gas. A sample mix containing bare DNA and reconstituted nucleosomes (usually 30%–50% of the DNA strands do not bind to histones) was incubated at 200 mM NaCl and 10 mM Tris-HCl (pH 7.6) for all measurements for 1 min on ice. The sample mix was then deposited on the poly-L-lysine-coated muscovite mica for 30 s and subsequently rinsed with 20 mL milliQ water before drying with a gentle stream of filtered N_2 gas. We have previously investigated the influence of the ionic strength of the buffer on nucleosome conformations using a similar assay (39). Here we focused on the effect of histone modifications and used the same buffer conditions throughout.

We used two different commercial AFM instruments for imaging. All AFM images were acquired in tapping mode at room temperature. One set of images was acquired on a Multimode VIII AFM (Bruker, Billerica, MA) using silicon tips (AC160TS; drive frequency, 300–350 kHz; tip radius, 7 nm; Olympus, Tokyo, Japan). Images were scanned over a field of view of 3 × 3 μm at 2,048 × 2,048 pixels with a scanning speed of 1 Hz. Independent measurement repeats were performed on a Nanowizard Ultraspeed 2 (JPK, Berlin, Germany) with silicon tips (FASTSCAN-A; drive frequency, 1,400 kHz; tip radius, 5 nm; Bruker). Here, images were scanned over a field of view of 6 × 6 μm at 4,096 × 4,096 pixels with a scanning speed of 1.5 Hz or over a field of view of 12 × 12 μm at 8,192 × 8,192 pixels at 1.5 Hz (Fig. 1 *b*). For each nucleosome type, five (four for H3S10phos) independent data sets were recorded. The nucleosome samples for each data set were prepared in independent nucleosome reconstitutions. The proteins that were used for the reconstitutions came from a total of two batches for each nucleosome type. Each data set corresponds to an AFM measurement run on a new mica sheet with multiple images recorded that contain a total of more than 1,000 nucleosomes per data set.

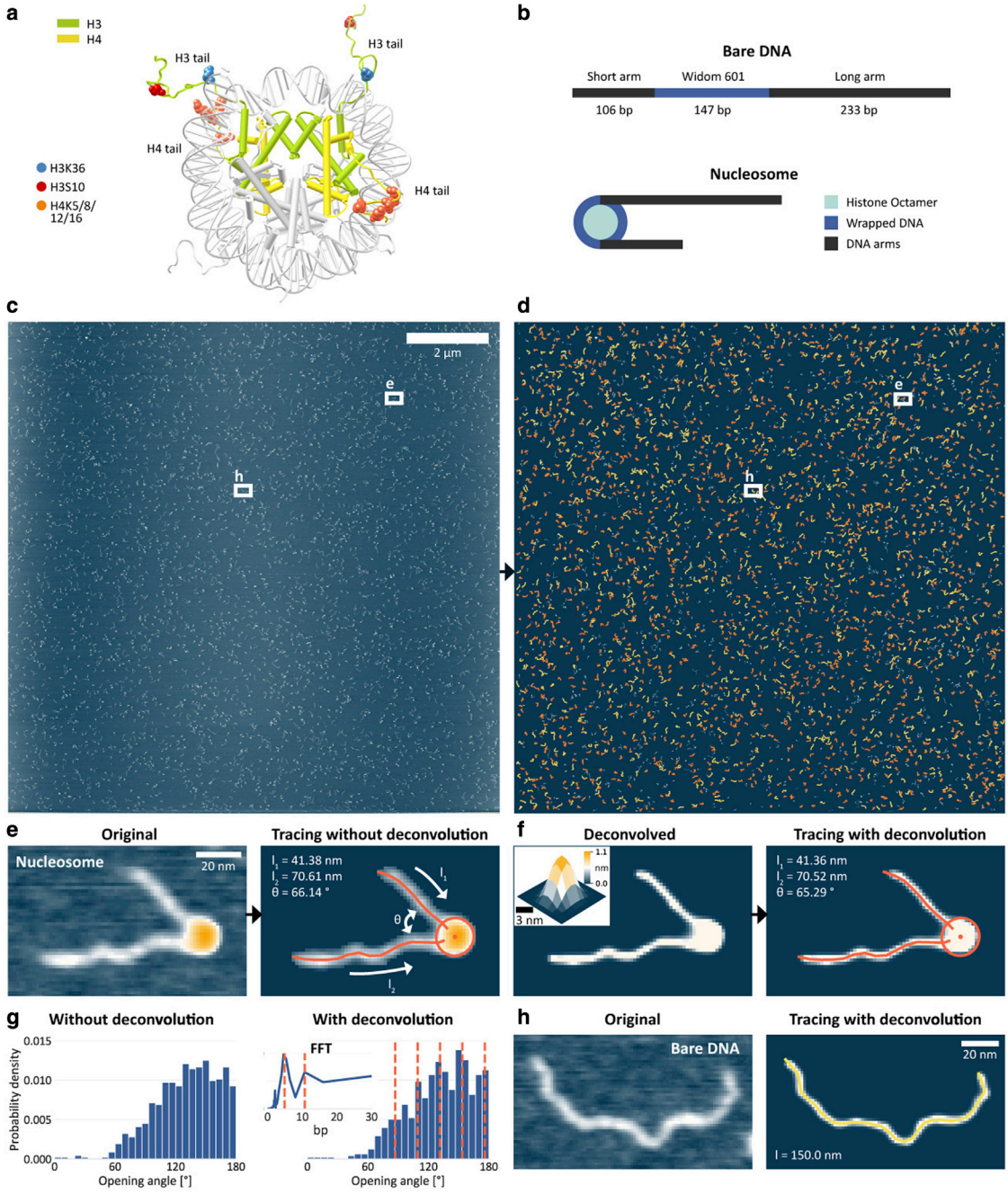

FIGURE 1 DNA and nucleosome structure parameters from automated AFM image analysis. (*a*) Crystal structure of a canonical nucleosome (PDB: 1KX5). Colored spheres represent the positions of the modified amino acids in the histone tail considered in this work. Among the three histone tail modifications investigated are three additional methyl groups at lysine 36 of histone H3 (H3K36me3, blue spheres), phosphorylation of H3 histones at serine 10 (H3S10phos, red spheres), and acetylation of H4 histones at lysines 5, 8, 12, and 16(H4K5/8/12/16ac, orange spheres). (*b*) Schematic of the construct used throughout this work. The 486-bp DNA consists of a 147-bp W601 nucleosome positioning sequence that is flanked by a short and a long arm of 106 bp and 233 bp, respectively. Histone octamers contain two copies each of H2A, H2B, H3, and H4. (*c*) AFM image of bare DNA and nucleosomes with a field of view of 12 × 12 µm at a resolution of 1.46 nm/pixel ($8{,}192^2$ pixels). (*d*) Traces of 901 bare DNA strands (orange) and 1,624 nucleosomes (yellow), obtained by the automated image analysis pipeline from the image shown in (*c*). (*e*) Magnification of a nucleosome image before and after tracing. The magnified area is indicated in (*c*) and (*d*). (*f*) Same nucleosome image as in (*e*) after Richardson-Lucy deconvolution. The inset displays the estimated shape of the AFM tip deduced from the bare DNA molecules in the same AFM image and used for deconvolution. (*g*) Opening angle distribution for the same data set, analyzed without and with deconvolution. The deconvolved data show the 20° (5-bp) unwrapping periodicity of nucleosomes ($N = 716$, only partially unwrapped nucleosomes are shown; see Fig. S3 for the same data set shown with different bin sizes). (*h*) Bare DNA before and after deconvolution and tracing.

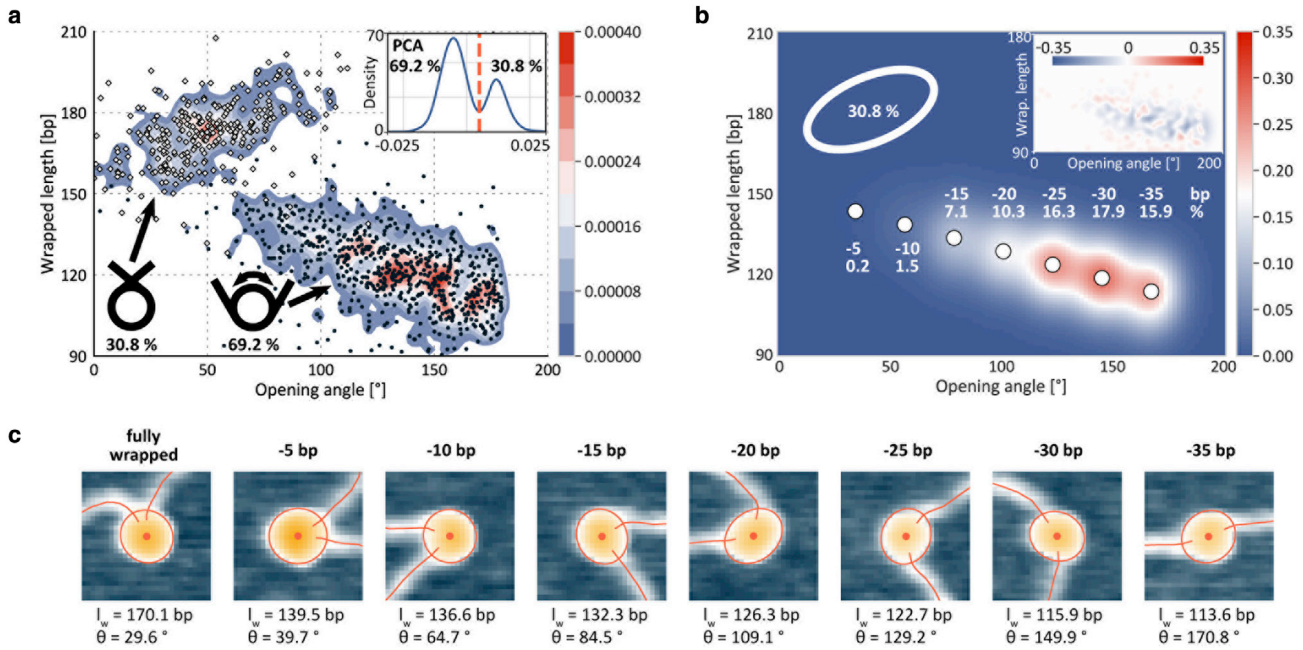

FIGURE 2 Estimating nucleosome wrapping populations. (*a*) Wrapped length versus opening angle distribution for canonical nucleosomes. White squares and black circles represent individual nucleosomes (N = 1,035), and the colored contours represent the 2D kernel density estimate (using a Gaussian kernel with bandwidth of 2.5°, 2.5 bp). The inset shows a principal-component analysis—a linear dimensionality reduction to 1D using singular value decomposition of the two parameters wrapped length and volume—that is used to separate the two nucleosome populations (fully versus partially wrapped). (*b*) 2D Gaussians fit to the density distribution of the partially unwrapped nucleosomes. The Gaussian amplitudes represent the populations of the 5-bp unwrapping substates; the inset shows the residuals of the fit to evaluate the quality of fitting. (*c*) Representative close-up shots of experimentally measured nucleosomes for the individual unwrapping states. Fully wrapped nucleosomes exceed the expected 147 bp of wrapping because of the overlapping of DNA at the entry/exit site, as described in the text.

AFM image analysis

To analyze the flattened AFM images, we used an analysis pipeline based in part on the previously published, open-source automated image analysis pipeline (39). In short, image analysis consists of three steps. First, molecules are detected and classified. For molecule detection, a Gaussian filter and a background subtraction are applied to the flattened AFM images, and then skeletonization (42), an algorithm that narrows down the objects to a one-pixel-wide backbone, is performed (Fig. S1). The skeleton of the molecules is used for classification. Bare DNA has exactly two endpoints in its skeleton and nucleosomes have exactly two endpoints and two branchpoints—points with more than two neighbors (Fig. S1). Second, a deconvolution is applied (see below). Third, the classified molecules are analyzed with respect to the structure parameters arm length, volume, and opening angle for nucleosomes and length for bare DNA (Fig. S1). Our AFM analysis code, including a detailed installation guide and an example image, is available at GitHub: https://github.com/SKonrad-Science/AFM_nucleoprotein_readout.

The populations of the individual unwrapping populations were determined by fitting seven two-dimensional (2D) Gaussians to the distributions of partially unwrapped nucleosomes as described in Fig. 2. The 2D Gaussians were initially centered at the positions expected from the 5-bp unwrapping periodicity and were allowed a maximum shift of 5 bp (for all Gaussians equally) on the wrapped length axis and no shift on the opening angle axis. The reasoning behind these values was the observation that angles are determined with the same accuracy for different data sets because of tip deconvolution, but the wrapped length can differ slightly in noisier images, and therefore fitting worked better when allowing this parameter to adapt slightly. The distances between the Gaussians were fixed, whereas the widths of the Gaussians were unconstrained in the fitting.

Image deconvolution

Image deconvolution is applied to the AFM images to more accurately trace nucleosomal opening angles and DNA length (Fig. 1). Before deconvolution can be performed, the point spread function, which is the result of a finite size AFM cantilever tip, must be estimated. The estimation is done for each AFM image individually because the tip shape can vary significantly even for tips of the same batch, and it can change while measuring one data set over the course of several hours. To estimate the tip shape, bare DNA strands are identified (see AFM image analysis) and traced without deconvolution to obtain an initial trace. Based on this initial trace, a grid of 11 × 11 pixels (∼15 × 15 nm) in size is filled by the height values surrounding the initial trace of the DNA strand (Fig. S2). This process is repeated for all DNA strands in the image and, by averaging the intensities in the grid, provides an estimate of the response of the tip to the cross section of a DNA molecule. Because the DNA width (∼2 nm) is less than the width of the tip (5–6 nm), we use this estimate as the point spread function for the deconvolution algorithm and refer to it as the "tip shape." Finally, we use the tip shape estimate and the Richardson-Lucy deconvolution algorithm (43,44), an iterative procedure for recovering an underlying image blurred by a known point spread function, to deconvolve the images. Using the bare DNA that is always present in our reconstituted nucleosome samples as a fiducial marker for estimating the tip shape is convenient because it avoids the need for preparation and co-deposition of additional control samples. DNA provides a highly reproducible and robust object of dimensions similar to the sample of interest; i.e., to the nucleosomes.

AFM image simulations

To simulate nucleosome images with different levels of anticooperative unwrapping, an 11-nm-diameter disk of uniform height together with

protruding DNA arms based on the worm-like chain model at opening angles deduced from the nucleosome crystal structure (PDB: 1KX5) was placed on a flat surface. The fully wrapped lengths of the short and long arms comprise 106 bp and 233 bp, respectively, and lengths were increased in 5-bp steps to simulate the individual unwrapping steps up to 35 bp. The simulated populations for each unwrapping state were chosen based on the experimentally determined populations. For simulation of anticooperative unwrapping, the length of only one arm was increased while keeping the length of the other arm constant. For simulation of stochastic unwrapping, the arms were unwrapped randomly in 5-bp steps up to the total amount of unwrapping simulated for each state. For example, when simulating a state of 10 bp unwrapped, possible lengths for the short arm are [106, 111, 116] bp and [233, 238, 243] bp for the long arm and were assigned randomly for each simulated nucleosome while keeping the total of 10 bp unwrapped between the two arms constant. Consecutively, the DNA arms were dilated to their expected with of 2 nm, and random noise in combination with a Gaussian filter ($\sigma = 2$ nm) was applied to mimic the effect of tip convolution. The simulation code is available at GitHub: https://github.com/SKonrad-Science/AFM_nucleoprotein_readout/ in the subfolder *artificial_image_simulation*.

RESULTS

Quantifying nucleosome conformations via automated AFM image analysis with deconvolution

We assembled nucleosomes by salt gradient dialysis under substoichiometric conditions so that the final sample contains bare DNA and predominantly mononucleosomes. We use a 486-bp DNA construct that features a W601 nucleosome positioning sequence (45) (147 bp) flanked by a short DNA arm (106 bp) and a long arm (233 bp) (Fig. 1 *b*; Materials and methods). We deposited samples from an aqueous buffer on poly-L-lysine-coated mica prior to rinsing and drying of the sample. High-resolution images of the deposited nucleosome samples were obtained by amplitude-modulation AFM in air (Fig. 1 *c*).

To quantify nucleosome conformations from the AFM images, we build on our previously published AFM image analysis pipeline to trace bare DNA and nucleosomes in the AFM images by multiparameter analysis (39) and extend it by adding a deconvolution step that allows more accurate tracing. The tracing consists of two steps. First, bare DNA and nucleosomes are detected and classified by subtracting the background and consecutively utilizing the topology of the one-pixel-wide backbone—the skeleton—of the molecules (Fig. S1). Second, structural parameters of the classified molecules are extracted by automatically tracing the molecules with the custom analysis software. The extracted parameters comprise contour length and bend angles for bare DNA and core particle height and volume, arm lengths, and opening angle for nucleosomes (Fig. 1, *e–h*). The vectors connecting the ends of the arm entry/exit region of the core particle and the center of the core particle define the nucleosome opening angle. In particular, the combined information of free DNA contour length and opening angle enables identification of the unwrapping state of each nucleosome; i.e., to classify how the DNA wraps around the histone core.

To increase the accuracy of our assay compared with previous applications of AFM imaging to nucleosome conformations, we implemented an image deconvolution step. In general, the dimensions of molecules are overestimated in AFM imaging because of the finite size of the AFM tip, which essentially acts as a point spread function (39,46). In particular, we find that tip convolution obscures the exact entry/exit position of DNA in the nucleosome images. We estimate the shape of the AFM cantilever tip (Fig. 1 *f*, inset; Fig. S2; Materials and methods) from the bare DNA in our images and typically find tip shape estimates with an end radius of 5–6 nm (Fig. 1 *f*, inset), in line with the size specified by the manufacturer (Materials and methods). Our algorithm, strictly speaking, not only estimates the AFM tip shape but a shape that is convolved with the finite thickness of the DNA strands. Because the width of DNA of ∼2 nm is considerably smaller than the estimated tip shape of 5–10 nm, we use this estimated shape as the point spread function in the deconvolution step and refer to it for simplicity as the tip shape. We use our tip shape estimate for subsequent image deconvolution based on the Richardson-Lucy algorithm (43,44) (Materials and methods). Applying the tip deconvolution leads to sharper images, in particular evident from the DNA paths (Fig. 1, *f* and *h*).

Comparing the opening angles measured with and without image deconvolution demonstrates the considerable effect of this approach (Fig. 1 *g*). Although the angle distribution of nucleosomes traced without deconvolution gives a broad and relatively featureless distribution of opening angles, the distribution of opening angles traced after applying the deconvolution clearly indicates a periodicity in the opening angle distribution of ∼20°; i.e., 5 bp of unwrapping (Fig. 1 *g*, inset; a fully wrapped nucleosome wraps 147 bp in ∼1.7 turns). This 5-bp unwrapping periodicity ultimately stems from the periodicity of the DNA helix and is in line with results from single-molecule DNA force spectroscopy experiments (47,48) and with cryoelectron microscopy (cryo-EM) observations of nucleosome wrapping states (49).

Quantifying nucleosome wrapping populations by multiparameter analysis

To quantify the length of DNA wrapped in the nucleosomes from AFM data, we evaluated the average contour length of the bare DNA molecules in each image (Fig. S3) and similarly measured the nucleosome arm lengths. By subtracting the combined arm lengths of individual nucleosomes from the mean contour length of bare DNA molecules, we obtain the wrapped length; i.e., the length of DNA confined in the nucleosome core particle. Simultaneously, we obtain the opening angle between the DNA segments entering the nucleosome particle for each nucleosome. The 2D

distribution of nucleosome opening angles and nucleosome wrapping provides a quantitative view of the nucleosome wrapping landscape (39) (Fig. 2). For a representative data set of canonical nucleosomes, the 2D kernel density distribution reveals two major populations (Fig. 2 *a*): one that features wrapped lengths greater than 150 bp and opening angles less than 100° and one that features wrapped lengths less than 150 bp and opening angles greater than 70°. We have previously identified (39) the population of nucleosomes with wrapped lengths of less than 150 bp as partially unwrapped. This population features a negative correlation between opening angle and wrapped length because the opening angle increases by further unwrapping of the DNA arms. Similarly, we have previously assigned the remaining population with wrapping of more than 150 bp of DNA to fully wrapped nucleosomes. Previous simulations of nucleosomes in AFM imaging (39) rationalize why the apparent wrapped lengths for fully wrapped nucleosomes exceed the 147 bp expected from the crystal structure: the DNA arms that leave the nucleosome entry/exit site overlap close to the nucleosome core particle. In the images, the crossing DNA strands lead to underestimation of the length of the DNA arms, resulting in longer apparent wrapped lengths for fully wrapped nucleosomes. Utilizing the local minimum seen in the principal-component analysis of nucleosome core volumes and opening angles (Fig. 2 *a*, inset), we separated fully wrapped and partially unwrapped nucleosomes (white and black dots, respectively) and find that, in this particular data set of unmodified nucleosomes, 31% of the nucleosomes are fully wrapped, and 69% of the nucleosomes are partially unwrapped.

To quantitatively investigate nucleosome unwrapping, we fitted the distribution of partially unwrapped nucleosomes with seven 2D Gaussians, one Gaussian per 5-bp unwrapping step up to an unwrapping of 35 bp, located at fixed distances with equal spacing of 5 bp and corresponding to the unwrapping periodicity (Fig. 2 *b*). The fitted amplitudes of the Gaussians represent the occupancies of the individual states of unwrapping and show that, for unmodified nucleosomes, most of the partially unwrapped nucleosomes unwrap 25–35 bp of DNA. To quantify how reproducibly our analysis pipeline can determine the wrapping populations, we performed independent repeat measurements, all from independent nucleosome reconstitutions and two protein batches (Materials and methods), and applied the same analysis pipeline to the separate data sets to obtain mean wrapping distributions and errors. Each repeat comprises more than 1,000 individual nucleosome molecules. Our method is highly reproducible and yields very precise estimates of the individual wrapping populations; the average absolute SEM for the populations is ∼1%. Therefore, our analysis pipeline provides a highly accurate and quantitative assay to investigate the effect of epigenetic modifications on nucleosome structure.

PTMs alter wrapping of H3K36me3 nucleosomes

To study how post-translational histone tail modifications affect nucleosome wrapping on the single-molecule level, we applied our analysis pipeline to two nucleosome constructs that have PTMs close to the DNA entry/exit region, H3K36me3 and H4K5/8/12/16ac, and one nucleosome construct that has a PTM farther outside of the nucleosome core particle at the end of the histone H3 tails, H3S10phos (Fig. 3). As for the unmodified nucleosomes, we performed 4–5 independent repeat measurements from independent nucleosome reconstitutions and two protein batches, all measured on different days for each nucleosome variant.

For H3K36me3 nucleosomes (i.e., nucleosomes with three methyl moieties on the ϵ amino group of lysine residue 36 of the histone H3 tails), we find that only a small fraction populates the fully wrapped state (16.5% ± 1.1%; mean +SE from five biological repeats compared with 31.2% ± 1.3% for canonical nucleosomes; Fig. 3 *a*) and that the vast majority of nucleosomes populates states of partial unwrapping (83.5% ± 1.1%). H3K36me3 nucleosomes are almost 2-fold less likely to occupy the fully wrapped state compared with canonical nucleosomes and are significantly more likely ($p = 0.005$ from a two-sample *t*-test) to populate states of higher unwrapping at −35 bp (Fig. 3 *c*). Thus, trimethylation at H3K36 alters the nucleosome structure toward increased unwrapping. Previous Förster Resonance Eenergy Transfer (FRET) studies did not find a measurable difference in nucleosome unwrapping between H3K36me3 and canonical nucleosomes (29,30). However, these studies rely on binding of the repressor protein LexA to the partially unwrapped nucleosomes between base pairs 8 and 27 and, thus, require a change in the states of unwrapping more than 25 bp to detect differences between H3K36me3 and canonical nucleosomes. Our data show that only part of the additionally unwrapped H3K36me3 nucleosomes populate these states of higher unwrapping, and, thus, the overall increased unwrapping might not be detected by the FRET/LexA methodology at the same level of detail as in our assay.

For H3S10phos nucleosomes (i.e., nucleosomes with phosphorylated histone tails at serine residue 10), we find no significant differences in partial unwrapping compared with canonical nucleosomes (two-sample *t*-test, $p = 0.13$). Of the phosphorylated nucleosomes, 28.1% ± 1.3% are fully wrapped, and 71.9% ± 1.3% are partially unwrapped. Phosphorylation introduces a negative charge to the serine and, thus, affects the electrostatic potential of the N-terminal histone tail. However, the modified serine lies on the outer end of the histone tail (Fig. 3 *b*), and, therefore, H3S10phos appears to have only a small effect on the intrinsic nucleosome structure, in line with a previous study that suggested that H3S10phos does not merely act by creating an open

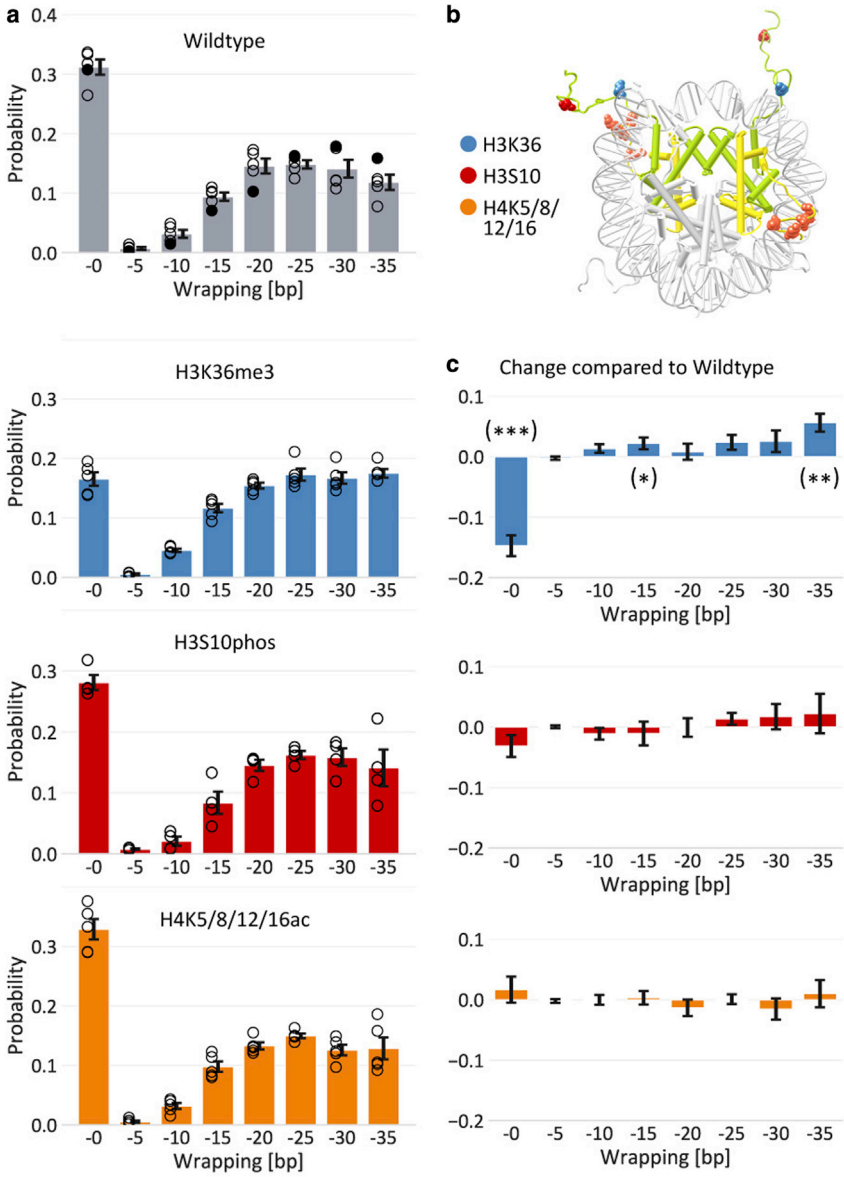

FIGURE 3 DNA wrapping populations of post-translationally modified nucleosomes. (*a*) Populations of DNA wrapping conformations for unmodified nucleosomes and the three modified nucleosome constructs containing H3K36me3, H3S10phos, or H4K5/8/12/16ac. The populations were determined from high-throughput analysis of AFM images, as shown in Fig. 2; the filled black circles in (*a*) are from the data set in Fig. 2. For each histone variant, four to five independent measurement repeats were obtained. Circles indicate the populations of the individual data sets and bars and error bars indicate the mean ± SE from the independent repeats. (*b*) Crystal structure of the canonical nucleosome (PDB: 1KX5). Colored spheres represent the positions of the modified histone tail amino acids. (*c*) Differences between the wrapping populations of the modified nucleosomes and the unmodified nucleosomes. Significant differences, as determined by two-sample *t*-tests, are indicated by 1,2 or 3 stars at the $p < 0.05$, < 0.01, and < 0.001 level, respectively.

chromatin configuration in which DNA is more accessible to the transcriptional machinery (50,51).

For H4K5/8/12/16ac nucleosomes (i.e., nucleosomes with acetylated histone H4 tails at lysine residues 5, 8, 12, and 16), we find that 32.9% ± 1.7% of the nucleosomes to occupy the fully wrapped state; 67.1% ± 1.7% occupy states of partial unwrapping, with most of them unwrapping 20–35 bp of DNA (Fig. 3 *a*), corresponding to no significant differences in wrapping between the tetraacetylated and canonical nucleosomes ($p = 0.46$; Fig. 3 *c*). Histone tail acetylations neutralize the positive charge of the modified lysines and, thus, reduce electrostatic interactions between the histone tails and the negatively charged DNA. Our observation for H4K5/8/12/16ac nucleosomes is in agreement with a recent single-molecule study that found no increased unwrapping for nucleosomes that contained 12 H4 tail lysine acetylation mimics—3-fold more than in our construct (31). Similarly, a FRET study found no effect of H4 acetylations on DNA entry/exit site geometry under the same ionic conditions as ours (52). We speculate that hydrogen bonding and hydrophobic forces outweigh electrostatic interactions in the binding between histone H4 tail lysines 5, 8, 12, and 16 and DNA, as proposed for H4K16 in a previous simulation study on the effect of H4K16ac on histone-DNA binding affinity (53).

PTMs can affect nucleosome unwrapping pathways

Previous studies based on single-molecule manipulation, FRET (54), and cryo-EM (49) revealed that unwrapping at one exit site stabilizes binding at the second exit site,

leading to anticooperative unwrapping of DNA from nucleosomes. We have shown recently that, by analyzing the distribution of short arm lengths versus opening angles, our high-throughput AFM image analysis approach is sensitive enough to detect this anticooperative unwrapping of canonical nucleosomes (39). In our data, the anticooperative opening of nucleosomes becomes apparent for the nucleosomes at opening angles greater than 80° (i.e., in the regimen of partially unwrapped nucleosomes); the population splits into two branches, indicating that unwrapping can follow two distinct pathways (Fig. 4 *a*). In the first pathway, the length of the short arm remains constant, whereas the opening angle increases, suggesting exclusive unwrapping of the long arm. In the second pathway, the length of the short arm increases linearly with the opening angle, consistent with exclusive unwrapping of the short arm (Fig. S4). The clearly separated pathways reflect the anticooperative nature of the unwrapping process (39).

To investigate the effect of epigenetic modifications on the cooperativity of nucleosome unwrapping, we calculate the probability of a certain nucleosome type to unwrap anticooperatively (Fig. S4). For this purpose, we define an area in the 2D opening angle versus short arm length density distribution (Figs. 4 *a* and S4), in which the nucleosomes are expected to lie in the case of anticooperative unwrapping (see Fig. S4 for more detailed information) and compare the population size with the fraction of nucleosomes outside of that area. For the canonical nucleosomes, 82.5% ± 0.8% (mean +SE from five biological repeats) are in the anticooperative unwrapping regimen. Similarly, the H3S10phos and H4K5/8/12/16ac nucleosomes occupy the anticooperative unwrapping regimen at 82.3% ± 1.4% and 81.3% ± 0.9%, respectively (Fig. 4 *c*), indicating that these modifications do not affect the anticooperativity in nucleosome unwrapping.

In contrast, we find a significant reduction in anticooperativity for unwrapping of H3K36me3 (73.4% ± 0.7%) compared with the canonical nucleosomes (two-sample *t*-test, $p = 3.5 \times 10^{-5}$), implying that a substantial part of H3K36me3 unwraps stochastically from both sides. Previously, we observed a similar effect (39) for nucleosomes that contained the histone H3 variant CENP-A (centromere protein A; Fig. 4 *c*). We speculated that the shortened N-terminal α helix (αN) of CENP-A nucleosomes, compared with the larger H3 αN of canonical nucleosomes, might cause the loss of anticooperativity, in line with a previous cryo-EM study that has suggested that allosteric changes involving H3 αN might invoke anticooperative unwrapping in canonical nucleosomes (49). Comparing our findings for H3K36me3 nucleosomes with the CENP-A data from the previous study shows a similar reduction of anticooperativity (Fig. 4 *b*) for both nucleosome types. Exchange of H3 with CENP-A and trimethylation at H3K36 introduce changes to the histone octamer at the entry/exit region of the DNA and a reduced fraction of fully wrapped nucleosomes. Our finding of reduced anticooperativity in

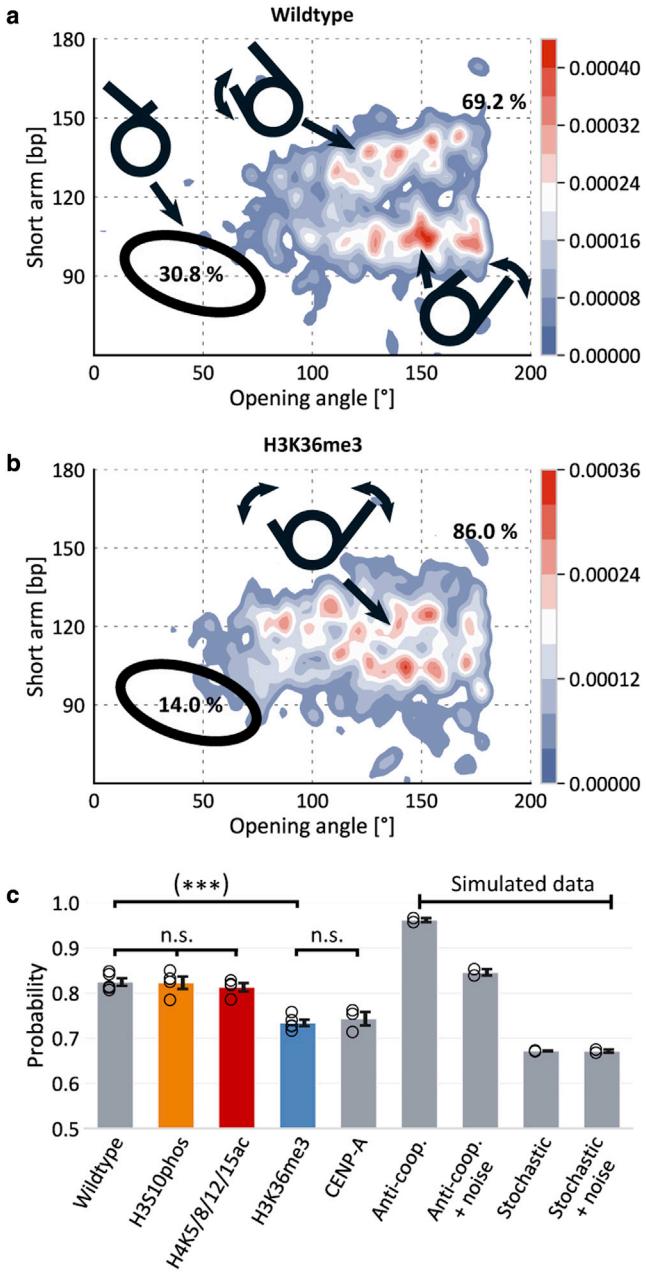

FIGURE 4 Unwrapping pathways of post-translationally modified nucleosomes. (*a*) 2D kernel density profile (bandwidth, 2.5°; 2.5 bp) of short arm length and opening angle for H3 nucleosomes. A bimodal distribution for opening angles greater than 80° is apparent, consistent with anticooperative unwrapping of the nucleosome core particle ($N = 1{,}035$). The distribution of fully wrapped nucleosomes (30.8% of all nucleosomes, indicated by the black ellipse) was omitted from the plot for clarity. (*b*) 2D kernel density profile (bandwidth, 2.5°; 2.5 bp) of short arm length and opening angle for H3K36me3 nucleosomes ($N = 1{,}155$). (*c*) Quantification of the tendency of the different epigenetically modified nucleosomes to unwrap anticooperatively or not (Fig. S4). Unmodified, H3S10phos, and H4K5/8/12/16ac nucleosomes show similar high levels of anticooperative unwrapping; in contrast, H3K36me3 and CENP-A nucleosomes unwrap less anticooperatively. Differences were tested for significance by two-sample *t*-tests: n.s. indicates no significant difference at the $p = 0.05$ level, three stars indicate $p < 0.001$.

unwrapping of H3K36me3 nucleosomes indicates that already subtle changes at the DNA entry/exit site of nucleosomes can strongly affect nucleosomal dynamics and opening pathways. The distributions of short arm length versus opening angle (Fig. 4, *a* and *b*) are dependent on proper nucleosome positioning at the W601 sequence as shifts of the histone octamer along the DNA strand changes the respective short arm and long arm lengths. To exclude that solely differences in positioning between unmodified and H3K36me3 nucleosomes cause the difference in anticooperativity, we compared the positioning of unmodified and trimethylated nucleosomes but found no differences (Fig. S5).

To further understand the nature and extent of anticooperative unwrapping, we simulated synthetic AFM images of nucleosomes that explored two extreme scenarios: exhibiting only anticooperative unwrapping or completely stochastic unwrapping (Fig. S6). In short, we placed a disk representing the nucleosome core particle on a surface and simulated protruding DNA arms with different lengths at opening angles, as deduced from the unwrapping state and the nucleosome crystal structure. The simulated populations of unwrapping are based on the experimentally determined unwrapping populations for unmodified nucleosomes (see Materials and methods and Fig. S6 for more details).

Applying our analysis pipeline to simulated nucleosome images that exhibit completely anticooperative unwrapping and contain no added noise, we find very high scores for anticooperative unwrapping, more than 95%, as expected. This value is higher than what we observe for any of the experimental conditions. However, when we add Gaussian noise with a width of 5 bp, corresponding to approximately one pixel in our AFM images and representative of our imaging noise, to the short arm length, we find anticooperativity values of 84% $\pm$ 0.7%, which are still slightly higher but close to the experimentally observed values for canonical, H3S10phos, and H4K5/8/12/16ac nucleosomes, suggesting that our data are consistent with these types of nucleosomes exhibiting almost perfect anticooperative unwrapping. Conversely, when we simulate nucleosomes that unwrap randomly from either site, we find anticooperativity scores of 67% $\pm$ 0.3%, essentially independent of whether noise is added to the images because of the already stochastic nature of the distribution (Fig. S6). The anticooperativity scores for the randomly unwrapping simulations are lower than any of the experimentally determined values but relatively close to values determined for the H3K36me3 and CENP-A nucleosome, suggesting that, although H3K36me3 and CENP-A unwrap mostly randomly, they appear to retain some anticooperativity.

CONCLUSIONS

Quantitative assessment of conformations of post-translationally modified nucleosomes is key to understanding the mode of operation of the histone code. PTMs can have many effects on chromatin structure, such as entry site unwrapping, nucleosome destabilization, chromatin fiber destabilization, and histone-histone destabilization (2,18,23). In this work, we utilized a high-throughput image analysis pipeline to study the effect of the PTMs H3S10phos, H3K36me3, and H4K5/8/12/16 on nucleosome structure and dynamics. From a multiparameter analysis of more than 25,000 nucleosomes, we obtain a comprehensive and quantitative view of the molecular ensembles, which, in turn, allows us to extract detailed information about nucleosome wrapping with as little as 1% uncertainty (SEM) for the populations of the individual unwrapping states.

The H3K36me3 modification exhibited the strongest effect on nucleosome wrapping, probably because of its location at the DNA entry/exit site of the nucleosome. Although we observed partial unwrapping of ~70% of the canonical nucleosomes, ~85% of H3K36me3 nucleosomes occupied states of partial unwrapping. Strikingly, in stark contrast to the anticooperative unwrapping of canonical nucleosomes, where unwrapping from one side inhibits unwrapping from the other, H3K36me3 nucleosomes tend to unwrap stochastically from both sides. H3K36me3 acts by recruiting a number of histone PTM binding domains (28) and is associated with DNA repair, alternative splicing, and transcription (2,55). Work in *Drosophila* suggests that H3K36me3 is enriched in gene bodies, in particular in the region of transcribed genes distal to the transcription start site (56,57). The increased propensity of H3K36me3 nucleosomes to partially unwrap suggests that H3K36me3 can directly affect higher-order chromatin structure by increasing the heterogeneity of nucleosome-nucleosome contacts as well as the effective nucleosome valency (12).

On the macromolecular level, histone tails play a key role in formation of higher-order chromatin structures (3). Acetylation of the histone tails inhibits folding of the nucleosome array in vitro (10), and elevated histone acetylations increase chromatin accessibility (58) and reduce clustering of nucleosomes (59) in vivo. Additionally, H4 acetylation blocks the interaction between the H4 tail and the acidic patch of adjacent nucleosomes and, thus, decreases internucleosomal interactions (60). However, on the single-molecule level, we found no significant changes in nucleosome accessibility because of the H4K5/8/12/16ac modification.

Similarly, although we did not see significant changes in nucleosome wrapping for H3S10phos nucleosomes compared with canonical nucleosomes, it has been shown previously that, in principle, phosphorylation can have significant effects on nucleosome dynamics (61). However, in that study, the phosphorylation occurred closer to the nucleosome dyad compared with the phosphorylation investigated in our study, which lies toward the end of the histone H3 tails. We speculate that H3S10phos acts predominantly by binding proteins with H3S10phos specificity (62,63), such as certain members of the 14-3-3 family, and

also via cross talk with other PTMs, such as blocking of H3K9ac (64,65) or promotion of H3K14ac (66).

Our results highlight how different PTMs involved in transcriptionally active chromatin act through a range of mechanisms. We show that our high-throughput, high-resolution pipeline can reveal the effects of subtle chemical modifications on nucleosome conformations. More broadly, our approach is readily applicable to other nucleosome modifications and variants as well as their interactions with binding partners.

SUPPORTING MATERIAL

Supporting material can be found online at https://doi.org/10.1016/j.bpj.2022.01.014.

AUTHOR CONTRIBUTIONS

All authors designed the research. S.F.K. performed the research, analyzed data, and wrote the manuscript with input from all authors.

ACKNOWLEDGMENTS

We thank Philipp Korber and Felix Müller-Planitz for help with initial nucleosome reconstitutions; Pauline Kolbeck, Tine Brouns, Wout Frederickx, Herlinde De Keersmaecker, Steven De Feyter, and Björn H. Menze for discussions and assistance with AFM imaging; and Thomas Nicolaus and Yi-Yun Lin for help with sample preparation. This work was funded by the Deutsche Forschungsgemeinschaft (DFG, German Research Foundation) through SFB863 – Project ID 111166240 (A11).

SUPPORTING CITATIONS

References (67,68) appear in the supporting material.

REFERENCES

1. Sadakierska-Chudy, A., and M. Filip. 2015. A comprehensive view of the epigenetic landscape. Part II: histone post-translational modification, nucleosome level, and chromatin regulation by ncRNAs. *Neurotox. Res.* 27:172–197.
2. Bowman, G. D., and M. G. Poirier. 2015. Post-translational modifications of histones that influence nucleosome dynamics. *Chem. Rev.* 115:2274–2295.
3. Baldi, S., P. Korber, and P. B. Becker. 2020. Beads on a string—nucleosome array arrangements and folding of the chromatin fiber. *Nat. Struct. Mol. Biol.* 27:109–118.
4. Luger, K., A. W. Mäder, …, T. J. Richmond. 1997. Crystal structure of the nucleosome core particle at 2.8 Å resolution. *Nature.* 389:251–260.
5. Richmond, T. J., and C. A. Davey. 2003. The structure of DNA in the nucleosome core. *Nature.* 423:145–150.
6. Ngo, T. T. M., and T. Ha. 2015. Nucleosomes undergo slow spontaneous gaping. *Nucleic Acids Res.* 43:3964–3971.
7. Miyagi, A., T. Ando, and Y. L. Lyubchenko. 2011. Dynamics of nucleosomes assessed with time-lapse high-speed atomic force microscopy. *Biochemistry.* 50:7901–7908.
8. Fierz, B., and M. G. Poirier. 2019. Biophysics of chromatin dynamics. *Annu. Rev. Biophys.* 48:321–345.
9. van Deelen, K., H. Schiessel, and L. de Bruin. 2020. Ensembles of breathing nucleosomes: a computational study. *Biophys. J.* 118:2297–2308.
10. Garcia-Ramirez, M., C. Rocchini, and J. Ausio. 1995. Modulation of chromatin folding by histone acetylation. *J. Biol. Chem.* 270:17923–17928.
11. Dorigo, B., T. Schalch, …, T. J. Richmond. 2003. Chromatin fiber folding: requirement for the histone H4 N-terminal tail. *J. Mol. Biol.* 327:85–96.
12. Farr, S. E., E. J. Woods, …, R. Collepardo-Guevara. 2021. Nucleosome plasticity is a critical element of chromatin liquid–liquid phase separation and multivalent nucleosome interactions. *Nat. Commun.* 12:1–17.
13. Arya, G., and T. Schlick. 2009. A tale of tails: how histone tails mediate chromatin compaction in different salt and linker histone environments. *J. Phys. Chem. A.* 113:4045–4059.
14. Collepardo-Guevara, R., G. Portella, …, M. Orozco. 2015. Chromatin unfolding by epigenetic modifications explained by dramatic impairment of internucleosome interactions: a multiscale computational study. *J. Am. Chem. Soc.* 137:10205–10215.
15. Bannister, A. J., and T. Kouzarides. 2011. Regulation of chromatin by histone modifications. *Cell Res.* 21:381–395.
16. Sinha, M., and C. L. Peterson. 2009. Chromatin dynamics during repair of chromosomal DNA double-strand breaks. *Epigenomics.* 1:371–385.
17. Almouzni, G., and H. Cedar. 2016. Maintenance of epigenetic information. *Cold Spring Harb. Perspect. Biol.* 8:a019372.
18. Cosgrove, M. S., and C. Wolberger. 2005. How does the histone code work? *Biochem. Cell Biol.* 83:468–476.
19. Mersfelder, E. L., and M. R. Parthun. 2006. The tale beyond the tail: histone core domain modifications and the regulation of chromatin structure. *Nucleic Acids Res.* 34:2653–2662.
20. Blakey, C. A., and M. D. Litt. 2015. Histone modifications-models and mechanisms. *In* Epigenetic Gene Expression and Regulation. Elsevier Inc., pp. 21–42.
21. Zhang, R., J. Erler, and J. Langowski. 2017. Histone acetylation regulates chromatin accessibility: role of H4K16 in inter-nucleosome interaction. *Biophys. J.* 112:450–459.
22. Nadal, S., R. Raj, …, B. G. Davis. 2018. Synthetic post-translational modification of histones. *Curr. Opin. Chem. Biol.* 45:35–47.
23. Rothbart, S. B., and B. D. Strahl. 2014. Interpreting the language of histone and DNA modifications. *Biochim. Biophys. Acta.* 1839:627–643.
24. Cosgrove, M. S., J. D. Boeke, and C. Wolberger. 2004. Regulated nucleosome mobility and the histone code. *Nat. Struct. Mol. Biol.* 11:1037–1043.
25. Tessarz, P., and T. Kouzarides. 2014. Histone core modifications regulating nucleosome structure and dynamics. *Nat. Rev. Mol. Cell Biol.* 15:703–708.
26. Li, B., M. Carey, and J. L. Workman. 2007. The role of chromatin during transcription. *Cell.* 128:707–719.
27. Kouzarides, T. 2007. Chromatin modifications and their function. *Cell.* 128:693–705.
28. Musselman, C. A., M. E. Lalonde, …, T. G. Kutateladze. 2012. Perceiving the epigenetic landscape through histone readers. *Nat. Struct. Mol. Biol.* 19:1218–1227.
29. Musselman, C. A., M. D. Gibson, …, T. G. Kutateladze. 2013. Binding of PHF1 Tudor to H3K36me3 enhances nucleosome accessibility. *Nat. Commun.* https://doi.org/10.1038/ncomms3969.
30. Gibson, M. D., J. Gatchalian, …, M. G. Poirier. 2017. PHF1 Tudor and N-terminal domains synergistically target partially unwrapped nucleosomes to increase DNA accessibility. *Nucleic Acids Res.* 45:3767–3776.
31. Bintu, L., T. Ishibashi, …, C. Bustamante. 2012. Nucleosomal elements that control the topography of the barrier to transcription. *Cell.* 151:738–749.

32. Komar, D., and P. Juszczynski. 2020. Rebelled epigenome: histone H3S10 phosphorylation and H3S10 kinases in cancer biology and therapy. *Clin. Epigenetics.* 12:1–14.
33. Hodges, C., L. Bintu, …, C. Bustamante. 2009. Nucleosomal fluctuations govern the transcription dynamics of RNA polymerase II. *Science.* 325:626–628.
34. Katan, A. J., R. Vlijm, …, C. Dekker. 2015. Dynamics of nucleosomal structures measured by high-speed atomic force microscopy. *Small.* 11:976–984.
35. Ordu, O., A. Lusser, and N. H. Dekker. 2016. Recent insights from in vitro single-molecule studies into nucleosome structure and dynamics. *Biophys. Rev.* 8:33–49.
36. Lyubchenko, Y. L. 2018. Direct AFM visualization of the nanoscale dynamics of biomolecular complexes. *J. Phys. D Appl. Phys.* 51:403001.
37. Brouns, T., H. D. Keersmaecker, …, W. Vanderlinden. 2018. Free energy landscape and dynamics of supercoiled DNA by high-speed atomic force microscopy. *ACS Nano.* 12:11907–11916.
38. Würtz, M., D. Aumiller, …, K. Rohr. 2019. DNA accessibility of chromatosomes quantified by automated image analysis of AFM data. *Sci. Rep.* 9:12788.
39. Konrad, S. F., W. Vanderlinden, …, J. Lipfert. 2021. High-throughput AFM analysis reveals unwrapping pathways of H3 and CENP-A nucleosomes. *Nanoscale.* 13:5435–5447.
40. Shlyakhtenko, L. S., A. Y. Lushnikov, and Y. L. Lyubchenko. 2009. Dynamics of nucleosomes revealed by time-lapse atomic force microscopy. *Biochemistry.* 48:7842–7848.
41. Krietenstein, N., C. J. Wippo, …, P. Korber. 2012. Genome-wide in vitro reconstitution of yeast chromatin with in vivo-like nucleosome positioning. *Methods Enzymol.* 513:205–232.
42. Zhang, T. Y., and C. Y. Suen. 1984. A fast parallel algorithm for thinning digital patterns. *Commun. ACM.* 27:236–239.
43. Richardson, W. H. 1972. Bayesian-based iterative method of image restoration. *J. Opt. Soc. Am.* 62:55–59.
44. Lucy, L. B. 1974. An iterative technique for the rectification of observed distributions. *Astron. J.* 79:745–754.
45. Lowary, P. T., and J. Widom. 1998. New DNA sequence rules for high affinity binding to histone octamer and sequence-directed nucleosome positioning. *J. Mol. Biol.* 276:19–42.
46. Heath, G. R., E. Kots, …, S. Scheuring. 2021. Localization atomic force microscopy. *Nature.* 594:385–390.
47. Dechassa, M. L., K. Wyns, …, K. Luger. 2011. Structure and Scm3-mediated assembly of budding yeast centromeric nucleosomes. *Nat. Commun.* 2:1–10.
48. Li, M., and M. D. Wang. 2012. Unzipping single DNA molecules to study nucleosome structure and dynamics. *In* Methods in Enzymology. Elsevier Inc..
49. Bilokapić, S., M. Strauss, and M. Halić. 2018. Histone octamer rearranges to adapt to DNA unwrapping. *Nat. Struct. Mol. Biol.* 25:101–108.
50. Soledad Ivaldi, M., C. S. Karam, and V. G. Corces. 2007. Phosphorylation of histone H3 at Ser10 facilitates RNA polymerase II release from promoter-proximal pausing in Drosophila. *Genes Dev.* 21:2818–2831.
51. Hartzog, G. A., and J. W. Tamkun. 2007. A new role for histone tail modifications in transcription elongation. *Genes Dev.* 21:3209–3213.
52. Gansen, A., K. Tóth, …, J. Langowski. 2015. Opposing roles of H3- and H4-acetylation in the regulation of nucleosome structure - a FRET study. *Nucleic Acids Res.* 43:1433–1443.
53. Potoyan, D. A., and G. A. Papoian. 2012. Regulation of the H4 tail binding and folding landscapes via Lys-16 acetylation. *Proc. Natl. Acad. Sci. U S A.* 109:17857–17862.
54. Ngo, T. T. M., Q. Zhang, …, T. Ha. 2015. Asymmetric unwrapping of nucleosomes under tension directed by DNA local flexibility. *Cell.* 160:1135–1144.
55. Wagner, E. J., and P. B. Carpenter. 2012. Understanding the language of Lys36 methylation at histone H3. *Nat. Rev. Mol. Cell Biol.* 13:115–126.
56. modENCODE Consortium, Roy, S., …, M. F. Lin 2010. Identification of functional elements and regulatory circuits by Drosophila modENCODE. *Science.* 330:1787–1797.
57. Kharchenko, P. V., A. A. Alekseyenko, …, D. Linder-Basso. 2011. Comprehensive analysis of the chromatin landscape in Drosophila melanogaster. *Nature.* 471:480–486.
58. Görisch, S. M., M. Wachsmuth, …, K. Rippe. 2005. Histone acetylation increases chromatin accessibility. *J. Cell Sci.* 118:5825–5834.
59. Nozaki, T., R. Imai, …, K. Maeshima. 2017. Dynamic organization of chromatin domains revealed by super-resolution live-cell imaging. *Mol. Cell.* 67:282–293.e7.
60. Dhar, S., O. Gursoy-Yuzugullu, …, B. D. Price. 2017. The tale of a tail: histone H4 acetylation and the repair of DNA breaks. *Philos. Trans. R. Soc. Lond. B Biol. Sci.* 372:20160284.
61. North, J. A., S. Javaid, …, M. G. Poirier. 2011. Phosphorylation of histone H3(T118) alters nucleosome dynamics and remodeling. *Nucleic Acids Res.* 39:6465–6474.
62. Macdonald, N., J. P. Welburn, …, A. L. Clayton. 2005. Molecular basis for the recognition of phosphorylated and phosphoacetylated histone H3 by 14-3-3. *Mol. Cell.* 20:199–211.
63. Sawicka, A., and C. Seiser. 2014. Sensing core histone phosphorylation - a matter of perfect timing. *Biochim. Biophys. Acta* https://doi.org/10.1016/j.bbagrm.2014.04.013.
64. Latham, J. A., and S. Y. R. Dent. 2007. Cross-regulation of histone modifications. *Nat. Struct. Mol. Biol.* 14:1017–1024.
65. Duan, Q., H. Chen, …, W. Dai. 2008. Phosphorylation of H3S10 blocks the access of H3K9 by specific antibodies and histone methyltransferase: implication in regulating chromatin dynamics and epigenetic inheritance during mitosis. *J. Biol. Chem.* 283:33585–33590.
66. Cheung, P., K. G. Tanner, …, C. D. Allis. 2000. Synergistic coupling of histone H3 phosphorylation and acetylation in response to epidermal growth factor stimulation. *Mol. Cell.* 5:905–915.
67. Rivetti, C., M. Guthold, and C. Bustamante. 1996. Scanning force microscopy of DNA deposited onto mica: equilibration versus kinetic trapping studied by statistical polymer chain analysis. *J. Mol. Biol.* 264:919–932.
68. Zettl, T., R. S. Mathew, …, J. Lipfert. 2016. Absolute intramolecular distance measurements with angstrom-resolution using anomalous small-angle X-ray scattering. *Nano Lett.* 16:5353–5357.